Solid State Nuclear Magnetic Resonance 84 (2017) 34–40

Contents lists available at ScienceDirect

Solid State Nuclear Magnetic Resonance

journal homepage: www.elsevier.com/locate/ssnmr

Optimisation of excitation schemes for ^{14}N overtone MAS NMR using numerically exact simulations

Andreas Brinkmann[a], Luke A. O'Dell[b,*]

[a] Measurement Science and Standards, National Research Council Canada, 1200 Montreal Road, M40, Ottawa, Ontario, Canada K1A 0R6
[b] Institute for Frontier Materials, Deakin University, Waurn Ponds Campus, Geelong, Victoria 3220, Australia

ARTICLE INFO

Keywords:
^{14}N solid-state NMR
Overtone spectroscopy
Excitation pulses
WURST pulses
Composite pulses

ABSTRACT

Numerically exact simulations of the ^{14}N overtone ($^{14}N^{OT}$) MAS NMR experiment are used to investigate the effects of the applied magnetic field strength as well as three types of excitation pulse. The results show that both the resolution and sensitivity of $^{14}N^{OT}$ MAS NMR increase linearly with the applied static magnetic field strength. Standard RF excitation pulses are compared with frequency-swept WURST pulses as well as several composite pulses. WURST pulses are demonstrated to provide the largest bandwidths, while the direction of the frequency sweep is shown to be important when these pulses are used for the direct observation of $^{14}N^{OT}$ signals. A composite pulse is shown to provide the most efficient excitation overall, but only when applied on resonance. WURST excitation pulses are therefore the best option when studying a sample with unknown ^{14}N NMR parameters.

1. Introduction

Due to the large quadrupolar interaction and relatively low resonance frequency of the 99.6% natural abundance ^{14}N isotope, its Δm=2 transition can be directly excited and observed [1]. This phenomenon is known as overtone spectroscopy, and its primary advantage over other ^{14}N solid-state NMR methods [2,3] is the lack of first-order quadrupolar broadening for this transition, which reduces the associated frequency range from MHz down to tens of kHz [4,5]. The resulting second-order ^{14}N overtone ($^{14}N^{OT}$) powder patterns can potentially be fully resolved depending on their isotropic chemical and quadrupolar shifts, while magic angle spinning (MAS) can provide further gains in sensitivity and resolution [6,7]. Polarisation enhancement using symmetry-based pulse sequences [8] or dynamic nuclear polarisation (DNP) [9] can boost the signal strength, while more advanced rotation techniques such as double rotation (DOR) can further narrow the line widths [10]. The possibility of indirect detection via more amenable spin-half nuclei using pulse sequences such as HMQC [11–13] has also been investigated and the combination of this approach with DNP would seem to be the most promising method currently available for observing ^{14}N NMR signals in the solid state [9,14–17].

Despite the high natural abundance, $^{14}N^{OT}$ signal strengths are relatively weak and optimising the excitation of the overtone transition is crucial in both the direct and indirect observation cases. As the effective RF field experienced by this transition is scaled down relative to the fundamental transitions by a factor on the order of C_Q/ν_0 (where C_Q is the quadrupolar coupling constant and ν_0 is the ^{14}N Larmor frequency), long RF pulse lengths are generally required and these have correspondingly narrow excitation bandwidths. WURST pulses, which use a quadratic phase modulation to achieve a linear sweep of their effective frequency [18,19] have been proposed to overcome this issue and result in significant improvements in bandwidth for both direct [6] and indirect $^{14}N^{OT}$ excitation [15,17] under MAS. Various composite pulses have also been shown to provide improvements in both direct [20] and indirect $^{14}N^{OT}$ experiments [21]. In developing generally-applicable excitation schemes, an additional problem arises from the C_Q-dependence of the effective RF field, which makes it difficult to optimally excite multiple $^{14}N^{OT}$ signals from different nitrogen environments with a single pulse.

In this contribution, we have simulated a variety of $^{14}N^{OT}$ excitation pulses, comparing the performance of standard, WURST and composite pulses under MAS conditions. As previously published theoretical descriptions of $^{14}N^{OT}$ MAS NMR do not appear to fully agree with experimental data [22–24], we have used numerically exact simulations. Such calculations are relatively time consuming, but make no assumptions or simplifications and have previously been shown to provide very close agreement with observed results [7,15,17]. We have also used these simulations to investigate how the sensitivity and resolution of $^{14}N^{OT}$ MAS NMR varies with the applied magnetic field

* Corresponding author.
E-mail address: luke.odell@deakin.edu.au (L.A. O'Dell).

http://dx.doi.org/10.1016/j.ssnmr.2016.12.006
Received 27 October 2016; Received in revised form 8 December 2016; Accepted 8 December 2016
Available online 10 December 2016

strength.

2. Simulation details

The $^{14}N^{OT}$ MAS NMR simulations were carried out using the SpinDynamica code running in Mathematica. A full description of the simulation methods has been published previously along with example notebooks [7]. The simulations make use of the full time-dependent nuclear spin Hamiltonian including the Zeeman interaction, quadrupolar interaction and RF field. Two nitrogen environments were separately considered with C_Q values of 1 and 3 MHz to act as models for protonated primary amine (C-NH_3^+) and secondary amine (C-NH-C) groups respectively. In both cases the isotropic chemical shift, chemical shift anisotropy and quadrupolar asymmetry parameter were all set to zero. Magic angle spinning conditions were simulated with a sample rotation frequency of ν_R=+100 kHz. The COMPUTE algorithm [25] was used with the number of calculation points per rotor period manually adjusted to avoid the overlap of the fundamental and overtone ^{14}N signals, and all reported relative signal intensities and amplitudes have been corrected for this quantity. For $^{14}N^{OT}$ MAS NMR experiments, the dominance of the $+2\nu_R$ overtone sideband has been well-established [7,15] and only this signal is considered herein with the RF pulses applied on resonance unless otherwise stated. As $^{14}N^{OT}$ nutation frequencies are both C_Q-dependent and difficult to measure experimentally, the simulated RF field strength was set such that $\nu_1(^2H)$=100 kHz. For the results in Figs. 1–4 and 6, powder averaging was achieved using 144 or 300 crystallite orientations selected using the ZCW method [26], and 500 Hz of exponential line broadening was applied to each calculated FID prior to a Fourier transformation and manual phase correction. For Fig. 5, integration of the signal amplitudes was performed directly on the stick spectra calculated by COMPUTE before conversion into a conventional NMR spectrum.

Additional simulations were carried out to determine the maximum signal intensity that can be excited from the fundamental ^{14}N transitions at 100 kHz MAS for each nitrogen site. Standard pulses were applied on resonance with the central MAS band at $\nu_1(^2H)$=100 kHz and the optimum pulse lengths were determined using SIMPSON [27] as 0.9 μs for the C_Q=1 MHz site and 0.3 μs for the C_Q=3 MHz site. These pulse lengths were then used in the SpinDynamica calculations in order to directly compare the resulting signal intensities (summed integral of all sidebands) with those from the overtone transitions.

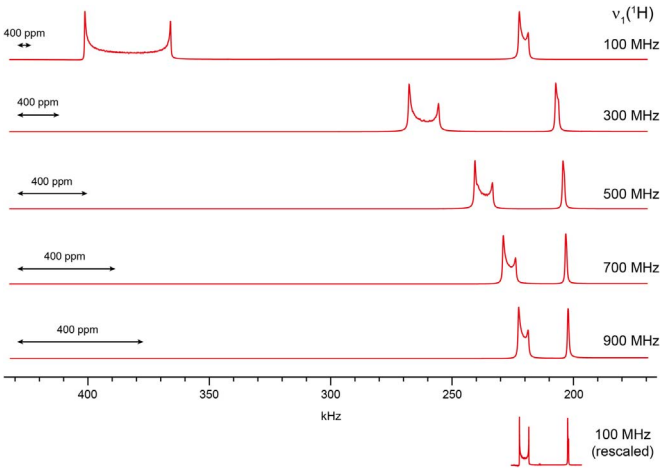

Fig. 1. Simulated $^{14}N^{OT}$ MAS NMR spectra featuring powder patterns from nitrogen sites with C_Q values of 3 and 1 MHz (left and right signals respectively) at different applied magnetic field strengths as indicated. A 400 ppm scale bar is shown to the left in each case. The spectrum at the bottom right has been rescaled horizontally by a factor of 1/9.

3. Results and discussion

3.1. Standard RF pulses and magnetic field dependence

Fig. 1 shows the simulated $^{14}N^{OT}$ MAS NMR spectra for the two nitrogen sites (C_Q=1 and 3 MHz) at applied magnetic field strengths ranging from $\nu_0(^1H)$=100–900 MHz. In this figure the individual $^{14}N^{OT}$ powder patterns were simulated separately and their heights normalised for visual comparison. A short pulse length of 1 μs was used in these simulations in order to minimise distortions to the powder pattern shapes, which can occur at longer pulse lengths. The powder pattern from the C_Q=3 MHz site is broader and located at a higher frequency due to its larger second-order quadrupolar interaction and isotropic quadrupolar shift respectively. As the applied magnetic field strength increases, both of these quantities decrease together in a linear fashion. As a result, the spectral resolution (which can be quantified as the separation of the powder patterns divided by their width) remains constant. This is illustrated by the 100 MHz spectrum shown at the bottom right, which after rescaling horizontally by a factor of 1/9 lines up perfectly with the 900 MHz spectrum (note that the difference in "sharpness" between these two spectra results only from the fact that the applied line broadening is also scaled). As these simulations do not include the effects of chemical shifts, which in terms of absolute frequency will increase linearly with B_0 and will act to spread out the range of $^{14}N^{OT}$ signals, it can be concluded that the inherent resolution of $^{14}N^{OT}$ MAS NMR spectra increases linearly with the applied magnetic field strength. This is illustrated by the increasing size of the 400 ppm scale bars in Fig. 1, 400 ppm being the approximate chemical shift range for nitrogen.

The optimum on-resonance RF pulse lengths (at $\nu_1(^2H)$=100 kHz) were determined for each nitrogen site as a function of magnetic field strength (Fig. 2a) by simulating various pulse durations and fitting the resulting integrated signal intensities to a sine function. As expected given the C_Q/ν_0 RF scaling factor discussed in the introduction, the C_Q=1 MHz site requires longer excitation pulse lengths, and for both C_Q values the optimum pulse lengths increase linearly with the applied field. The ratio of optimum pulse lengths for the two nitrogen sites is equal to 3.4 ± 0.1. The fact that this ratio is not exactly 3 may be due to the differences in powder pattern widths that would amplify any off-resonance effects for the C_Q=3 MHz signal, as well as the additional dependence of the effective RF field on the orientation of each individual crystallite, which causes the nutation frequency to vary across the line shape. The latter effect results in $^{14}N^{OT}$ powder patterns that become increasingly distorted in appearance as the pulse length is increased, a phenomenon that is more noticeable for the broader C_Q=3 MHz powder pattern. Over the entire range of applied magnetic field strengths, the optimum pulse lengths have excitation bandwidths (given approximately by the inverse of their durations) that are insufficient to cover the full spectral range and excite both nitrogen sites. In the following sections, WURST pulses and composite pulses are tested as potential ways to overcome this bandwidth issue.

The C_Q/ν_0 factor can also be used to quantify the size of the $^{14}N^{OT}$ signal that can be excited, relative to that which can (in theory) be excited from the fundamental transitions [23]. As the applied magnetic field increases, the excitation of the $^{14}N^{OT}$ transition becomes less efficient and the total $^{14}N^{OT}$ signal intensity excited by an optimised on-resonance RF pulse decreases (Fig. 2b). Regarding the fundamental transitions, in practice the large first-order quadrupolar broadening spreads out these transitions over frequency ranges of several MHz, meaning that they cannot be efficiently excited using a standard RF pulse. We simulated the maximum signal intensities excited from the fundamental transitions using optimised RF pulses applied to the central MAS band. As the Boltzmann polarisation was not taken into account in these simulations, these intensities are independent of the applied magnetic field strength. More signal intensity can excited from the fundamental transitions of the C_Q=1 MHz nitrogen site (approxi-

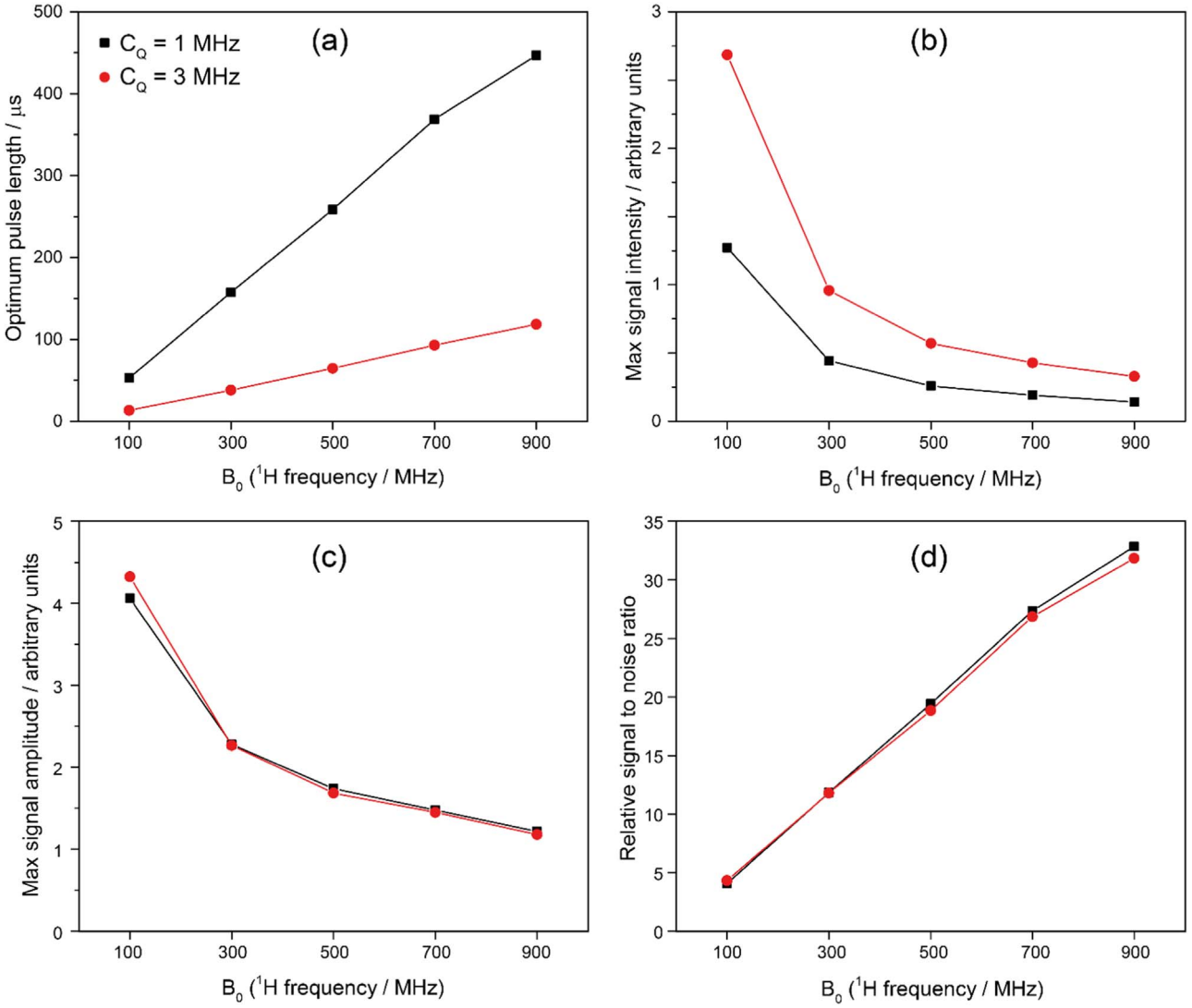

Fig. 2. Various simulated quantities plotted as a function of the applied magnetic field for the C_Q=1 and 3 MHz nitrogen sites (black squares and red circles respectively): (a) optimum pulse lengths, (b) maximum integrated signal intensities, (c) maximum signal amplitudes and (d) predicted relative signal-to-noise ratios. The latter quantities were calculated by rescaling the data in (c) by $B_0^{1.5}$ to account for experimental factors (see text for discussion). (For interpretation of the references to color in this figure legend, the reader is referred to the web version of this article.)

mately 9.6 at all fields, using the same intensity scale as Fig. 2b) than for the C_Q=3 MHz nitrogen site (approximately 3.2) due to the smaller first-order quadrupolar broadening in the former case. Note that these numbers correspond to the sum of all sideband intensities. In both cases, and at all applied fields, these intensities are significantly higher than those obtained from the optimal excitation of the overtone transition.

Interestingly, when the $^{14}N^{OT}$ signal amplitude (i.e., maximum peak height) is considered rather than the signal intensity (peak area), the two nitrogen sites show almost identical values (Fig. 2c). This is due to the fact that as C_Q increases, the spreading out of the signal by the second-order quadrupolar broadening is compensated for by the increasing total signal intensity due to the C_Q/ν_0 factor. The signal amplitudes shown in Fig. 2c, however, do not take into account certain additional effects that will alter the experimental sensitivity. Chief among these is the increasing Boltzmann polarisation that will scale linearly with B_0. To predict the experimental sensitivity in terms of a relative signal-to-noise ratio (S/N), we have corrected for this Boltzmann factor, as well as for the fact that the current induced in the RF coil increased linearly with B_0 (principle of reciprocity [28]) while the noise amplitude only increases as $B_0^{0.5}$. Thus, after rescaling the data in Fig. 2c by $B_0^{1.5}$, the anticipated S/N of the $^{14}N^{OT}$ MAS NMR experiment is shown to increase linearly with the applied magnetic field strength (Fig. 2d). $^{14}N^{OT}$ MAS NMR will therefore benefit from higher magnetic fields in terms of both resolution and sensitivity, although these advantages will be accompanied by the need for either longer excitation pulse lengths or stronger RF fields.

Below, we investigate the bandwidth performance of various RF pulse types, distinguishing between the excitation of only the C_Q=3 MHz powder pattern and the more challenging simultaneous excitation of both signals. For the latter case, simulations were carried out for the C_Q=1 and 3 MHz nitrogen environments with the transmitter frequency set to the midpoint between the outermost edges of the two $^{14}N^{OT}$ powder patterns. For these and all subsequent simulations, an intermediate value for the applied magnetic field strength of 11.7 T ($\nu_0(^1H)$=500 MHz) was chosen. Fig. 3a shows the resulting integrated intensities for the two nitrogen sites as a function of pulse length for a standard RF pulse applied at the centre of the spectrum. In this case, the optimum pulse duration for the simultaneous observation of both signals is around 30 μs, with a bandwidth of around 35 kHz sufficient to cover both peaks.

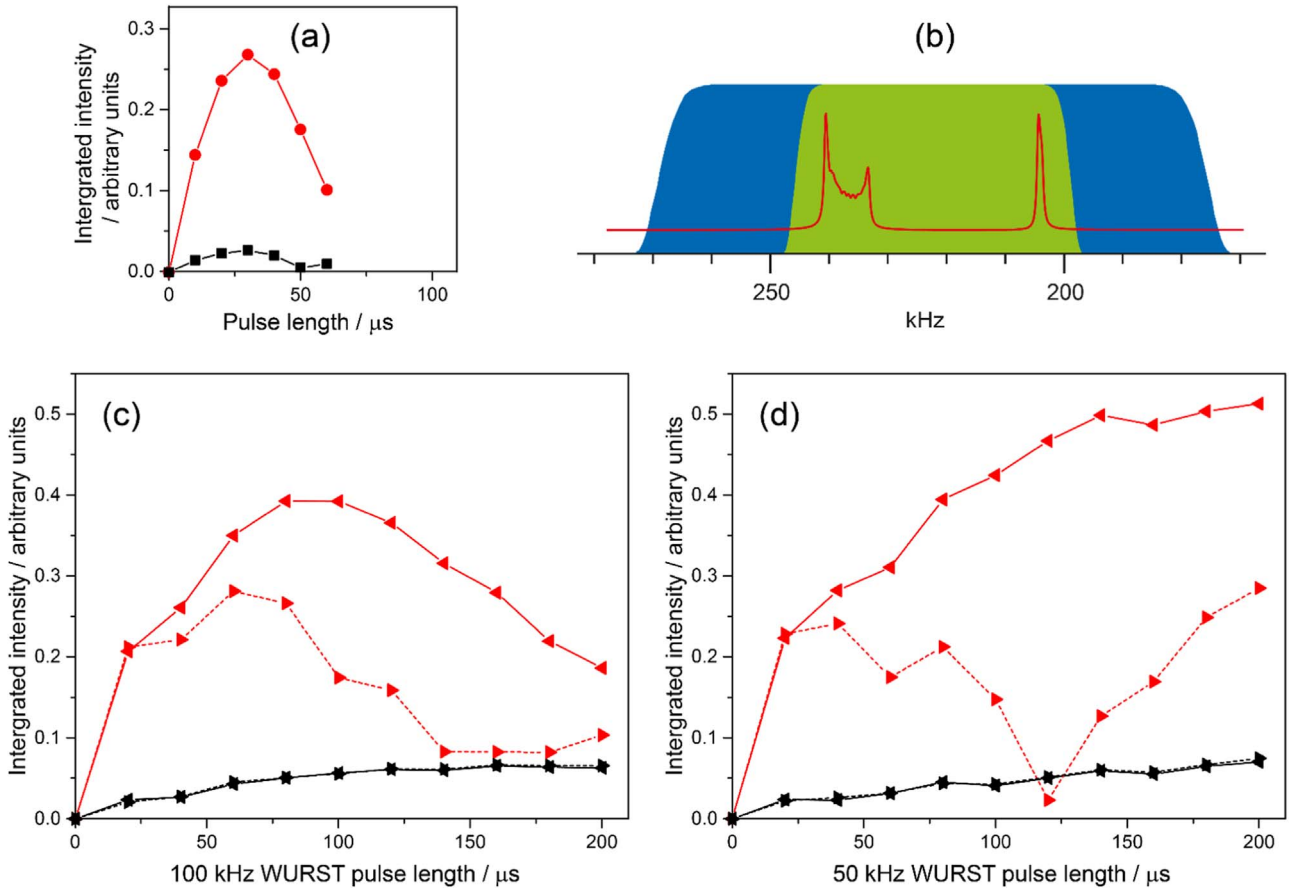

Fig. 3. (a) $^{14}N^{OT}$ MAS NMR signals (11.7 T, ν_R=+100 kHz and $\nu_1(^2H)$=100 kHz) excited by a standard RF pulse applied at the mid-point of the two signals (C_Q=1 MHz black squares and C_Q=3 MHz red circles). (b) Illustration of WURST-80 excitation pulses with sweep ranges of 100 kHz (blue) and 50 kHz (green) shown relative to the $^{14}N^{OT}$ spectrum. (c) and (d) show the integrated intensities resulting from the 100 kHz and 50 kHz sweep WURST pulses respectively (C_Q=1 MHz black triangles and C_Q=3 MHz red triangles). The triangles pointing to the left represent a sweep from low to high frequencies, and vice versa. The plots in (a), (c) and (d) are shown with the same vertical scale. (For interpretation of the references to color in this figure legend, the reader is referred to the web version of this article.)

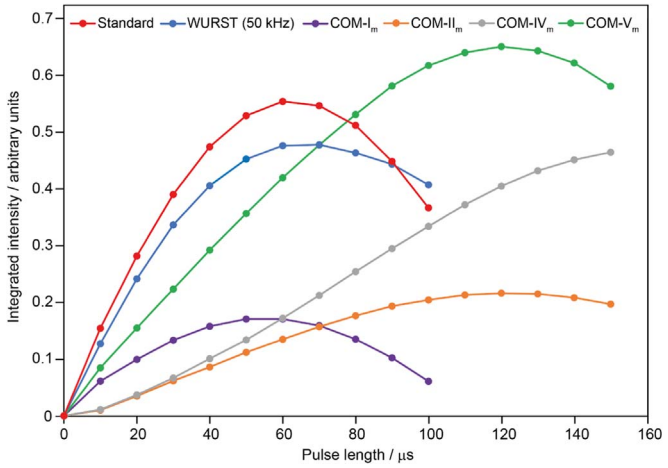

Fig. 4. (Color version available in web version.) Simulated $^{14}N^{OT}$ signal intensities produced by various pulse types as indicated, applied on-resonance with the C_Q=3 MHz nitrogen site (11.7 T, ν_R=+100 kHz and $\nu_1(^2H)$=100 kHz). Details of the four composite pulses can be found in Ref. [21].

3.2. WURST pulses

WURST pulses have already been demonstrated experimentally to exhibit broader $^{14}N^{OT}$ excitation profiles than standard RF pulses [6]. Their improved bandwidths stem from the linear sweep of their effective frequency over an arbitrary range. In this work we have tested two WURST excitation pulses with sweep ranges of 50 and 100 kHz. Both of these ranges are sufficient to cover the two $^{14}N^{OT}$ powder patterns as shown in Fig. 3b. In addition to the frequency sweep range, the direction of the frequency sweep must be specified, and this can have a significant effect when WURST excitation pulses are employed for the direct detection of $^{14}N^{OT}$ spectra.

Figs. 3c and d show the $^{14}N^{OT}$ signal intensities excited by WURST pulses with 100 kHz and 50 kHz sweep ranges respectively. As above, the red data points correspond to the C_Q=3 MHz site while the black points represent the C_Q=1 MHz site. The directions in which the triangles point represent the frequency sweep directions across the spectrum shown in Fig. 3b. The advantages of WURST pulses over standard RF pulses are clearly illustrated, with WURST pulses between 100 and 200 μs in length capable of exciting the two $^{14}N^{OT}$ signals far more effectively than the 30 μs standard pulse. Another significant observation is that the direction of the frequency sweep greatly affects the net signal observed from the broader (C_Q=3 MHz) $^{14}N^{OT}$ powder pattern. This can be easily understood. As the WURST pulses sweep across the spectrum they will excite the two $^{14}N^{OT}$ signals sequentially. When the sweep direction is from high to low frequency (i.e., left to right in Fig. 3b) the broader powder pattern will be excited at an earlier time than the narrower one, and since the acquisition of the time-domain signal does not begin until the sweep has finished, a significant fraction of this signal will be lost over the remaining pulse duration due to dephasing as a result of the second-order quadrupolar interaction. This is less of an issue for the C_Q=1 MHz signal due to the smaller interaction and correspondingly slower signal decay in the time domain, which is why the sweep direction makes little difference for

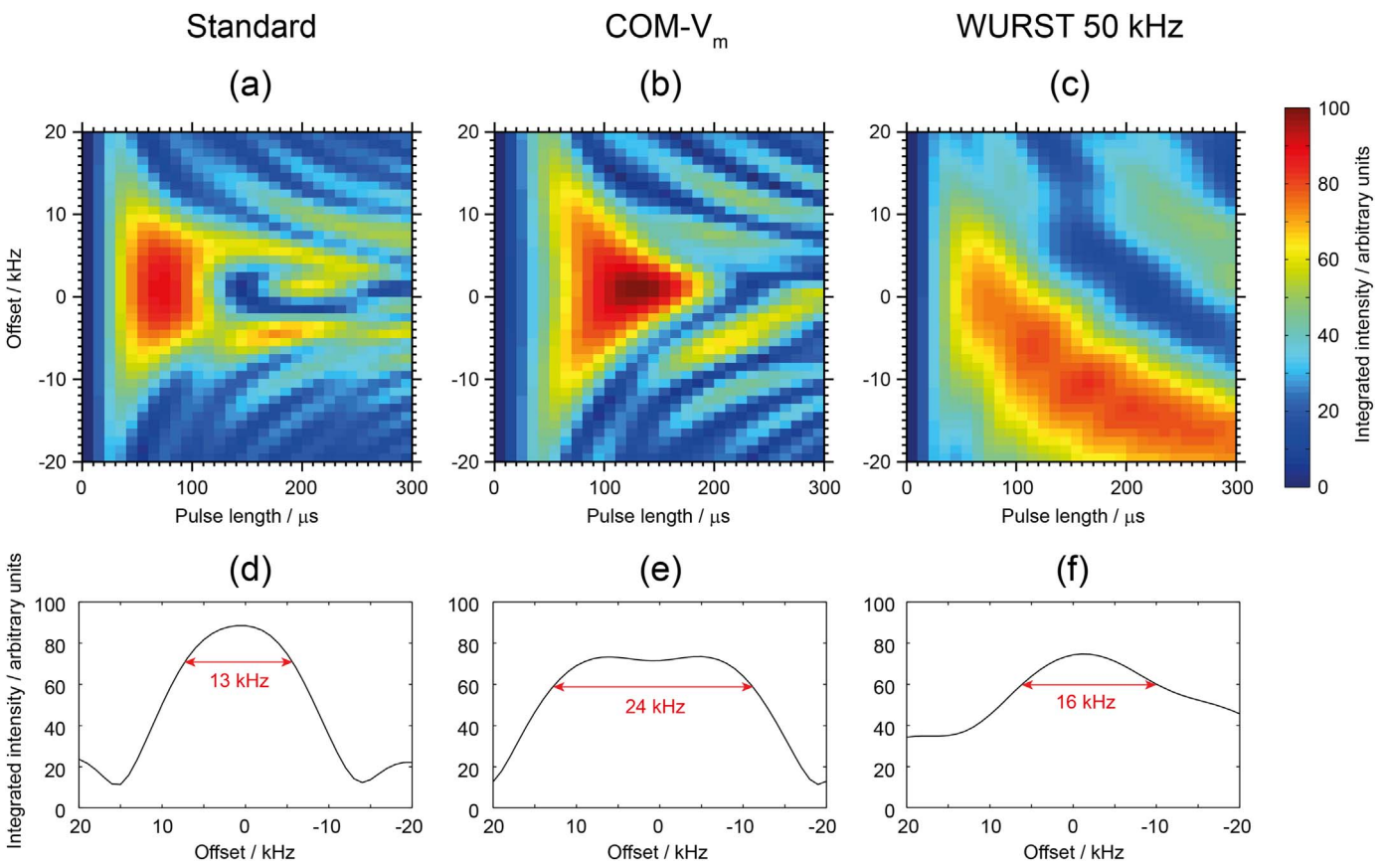

Fig. 5. Simulated $^{14}N^{OT}$ signal intensities produced from the C_Q=3 MHz site (11.7 T, ν_R=+100 kHz and $\nu_1(^2H)$=100 kHz) by three types of RF pulses as a function of pulse length and RF offset: (a) standard RF pulse, (b) COM-V_m pulse and (c) WURST pulse with 50 kHz sweep range. (d), (e) and (f) respectively show their excitation profiles for a pulse length of 70 μs, and the red lines indicate the bandwidths at 80% of the maximum signal intensity. (For interpretation of the references to color in this figure legend, the reader is referred to the web version of this article.)

that site. The broader $^{14}N^{OT}$ MAS NMR powder patterns will generally be located at higher frequencies due to their larger isotropic quadrupolar shifts (although this effect will become less significant at higher magnetic fields as the isotropic chemical shifts begin to dominate). Thus, in general, $^{14}N^{OT}$ WURST excitation pulses should be applied with sweep directions from low to high frequencies. Note that this conclusion only applies to "WURST pulse→acquire" experiments. When $^{14}N^{OT}$ WURST pulses are used in indirect detection pulse sequences such as HMQC, the sweep direction of the first pulse does not matter as long as it is reversed for the second pulse [15].

The optimum WURST pulse length is difficult to establish based on these simulations alone due to the time-dependent excitation and dephasing issue discussed above. The plot in Fig. 3d shows how the amount of signal generated by a WURST excitation pulse with a 50 kHz sweep continues to increase as the pulse length reaches 200 μs. However, the resulting C_Q=3 MHz powder pattern also becomes increasingly distorted away from its ideal shape as the pulse duration increases. From our simulations, a pulse length of around 100 μs appears to be a good compromise between maximising the excitation efficiency and minimising these distortions. Once again, note that this only applies to pulse→acquire experiments. In the case of indirect detection experiments such as ^1H-$^{14}N^{OT}$ HMQC, the dephasing issue will be absent and longer pulse lengths will likely be beneficial.

Aside from the importance of the pulse length and sweep direction, the sweep range also affects the excitation efficiency of the WURST pulse, with the 50 kHz sweep range providing improved excitation for the C_Q=3 MHz nitrogen site at any particular pulse duration. This is because the narrower sweep range results in a slower sweep *rate*, meaning that the pulse spends more time on-resonance with the $^{14}N^{OT}$ peak and results in a larger nutation angle. The WURST sweep range should therefore ideally be set to a value just large enough to excite all of the $^{14}N^{OT}$ signals present. Of course, for a sample with unknown ^{14}N parameters this range will be also be unknown, in which case the sweep range can be set to a larger value to maximise the likelihood of covering all potential signals.

3.3. Composite pulses

In a recent experimental study [21], the performance of four composite pulses used in a ^1H-$^{14}N^{OT}$ HMQC pulse sequence was investigated and compared with both standard and WURST pulses. The WURST pulses were found to provide the broadest and most uniform bandwidth, however, the composite pulses showed superior sensitivity at certain specific frequency offsets, a fact that can be exploited when the pulses are placed at the midpoint between two $^{14}N^{OT}$ signals. However, the durations of the composite pulses used in the study were set to the optimal value determined for a standard RF pulse. We have therefore carried out simulations to determine the optimum lengths for these pulses when applied on-resonance with the C_Q=3 MHz $^{14}N^{OT}$ signal at 11.7 T. The results are presented in Fig. 4 alongside both a standard pulse and a WURST pulse with a 50 kHz sweep range. We use the same naming convention for the composite pulses as Ref. [21], and readers are referred to this paper for the specifics of these composite pulses. The COM-I_m composite pulse is seen to have an optimum pulse length very similar in duration to the standard pulse, and this can explain the good performance of this pulse in the previous study (see Fig. 2 in Ref. [21]). However, for the other three composite pulses the optimum total pulse duration is clearly much longer. The COM-V_m pulse in particular excites the highest signal intensity, outperforming even the standard RF pulse when applied on

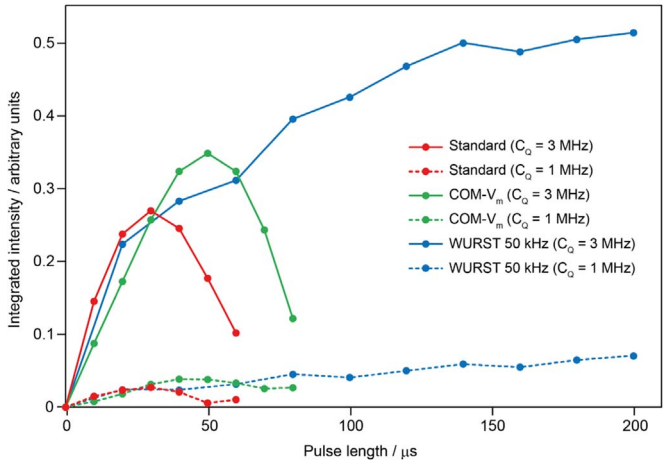

Fig. 6. (Color version available in web version.) Simulated $^{14}N^{OT}$ signal intensities produced by various pulse types as indicated (11.7 T, ν_R=+100 kHz and $\nu_1(^2H)$ =100 kHz), applied at the midpoint between the two nitrogen sites (C_Q=1 MHz dashed lines and C_Q=3 MHz continuous lines).

resonance. The optimum duration for this composite pulse is approximately double that of the standard pulse.

3.4. Bandwidth performance for a single nitrogen site

Fig. 5a shows the $^{14}N^{OT}$ integrated signal intensities after applying a standard RF pulse to the C_Q=3 MHz nitrogen site at 11.7 T, as a function of both the pulse length and RF offset. The maximum signal intensity is obtained on resonance with a pulse length of 70 μs. We can define the bandwidth of the pulse as the offset range in which the signal intensities remain above 80% of the maximum signal intensity. Using this definition we find the standard 70 μs pulse has a bandwidth of 13 kHz for the C_Q=3 MHz $^{14}N^{OT}$ signal (Fig. 5d).

A similar plot for the COM-V_m pulse is shown in Fig. 5b. As already mentioned in the previous section, this pulse gives the highest overall signal intensity of all the pulses studied when applied on resonance with a duration of 130 μs. However, at this particular pulse length the bandwidth of the COM-V_m pulse is only 7 kHz. At shorter pulse lengths the bandwidth improves significantly, and when applied with a duration of 70 μs, the COM-V_m bandwidth is 24 kHz (Fig. 5e), which is superior to that of the standard pulse albeit with a decrease in the overall excitation efficiency.

The same plot generated for the WURST pulse with a 50 kHz sweep range looks very different to that of the standard and composite pulses (Fig. 5c), with the efficiency skewed towards negative offsets as the pulse length is increased. This is due to the linear sweep of the pulse as discussed in Section 3.2. The sweep direction for the pulse in Fig. 5c is from low to high frequencies, thus for negative offsets the $^{14}N^{OT}$ powder pattern is excited at a later time and less signal is lost before the acquisition begins. The overall maximum signal intensity is found at a pulse length of 130 μs and an offset of −11 kHz, at which point the bandwidth as defined above is 12 kHz. This increases to 16 kHz for a WURST pulse length of 70 μs (Fig. 5f), a narrower bandwidth than that of the COM-V_m pulse with the same duration, although the WURST pulse does show better performance overall at larger offsets (± 20 kHz).

3.5. Bandwidth performance for multiple nitrogen sites

The simultaneous excitation of both the C_Q=1 and 3 MHz $^{14}N^{OT}$ signals is more challenging due to the increased bandwidth as well as the C_Q-dependent nutation rate. As shown in Fig. 1, at 11.7 T these two $^{14}N^{OT}$ powder patterns span a total frequency range of around 35 kHz. The excitation efficiencies of the various pulse types were therefore tested when applied at the midpoint of these two $^{14}N^{OT}$ signals. Of the four composite pulses, the COM-V_m pulse again showed the best performance, and is compared with a standard pulse and 50 kHz WURST pulse in Fig. 6 (for clarity the other three composite pulses are omitted from this figure). In agreement with the previous study [21], the COM-V_m pulse is superior to the standard pulse in terms of bandwidth and shows the best performance at a pulse length of 50 μs. However, at longer pulse durations, particularly above 100 μs, the WURST pulse outperforms both the standard and composite pulses with significantly more signal intensity excited from both nitrogen sites. These observations, along with the experimental work mentioned above [21], suggest that while composite pulses can provide the highest excitation efficiency when the locations of the $^{14}N^{OT}$ signals are known, WURST pulses remain the best option for the study of samples with unknown ^{14}N NMR parameters.

4. Summary

We have carried out a number of $^{14}N^{OT}$ MAS NMR simulations to study the effects of the applied magnetic field and the performance of three classes of excitation pulse. The results indicate that both the spectral resolution and sensitivity of the $^{14}N^{OT}$ MAS NMR experiment increase linearly with magnetic field strength, though these advantages come at a cost of increased RF pulse lengths/powers. At all fields, standard RF excitation pulses have insufficient bandwidth to excite the full potential range of $^{14}N^{OT}$ signals. WURST pulses provide dramatic increases in excitation bandwidth and can overcome this issue. When used as excitation pulses for the direct observation of $^{14}N^{OT}$ signals, the WURST pulse sweep direction should be from low to high frequencies to minimise the loss of signal from the broader $^{14}N^{OT}$ powder patterns. Finally, a composite pulse (COM-V_m) placed on resonance was found to show the highest excitation efficiency overall, but such pulses require advance knowledge of the $^{14}N^{OT}$ signal locations in order to be exploited, while WURST pulses are more suitable for samples with unknown ^{14}N NMR parameters.

Acknowledgements

SpinDynamica was programmed by Malcolm H. Levitt with contributions from Jyrki Rantaharju, Andreas Brinkmann and Soumya Singha Roy, and is available at http://www. SpinDynamica.soton.ac.uk.

References

[1] M. Bloom, M.A. LeGros, Can. J. Phys. 64 (1986) 1522–1528.
[2] L.A. O'Dell, Prog. Nucl. Magn. Reson. Spec. 59 (2011) 295–318.
[3] E. Dib, T. Mineva, B. Alonso, Ann. Rep. NMR Spec. 87 (2016) 175–235.
[4] R. Tycko, S. Opella, J. Am. Chem. Soc. 108 (1986) 3531–3532.
[5] R. Tycko, S. Opella, J. Chem. Phys. 86 (1987) 1761–1774.
[6] L.A. O'Dell, C.I. Ratcliffe, Chem. Phys. Lett. 514 (2011) 168–173.
[7] L.A. O'Dell, A. Brinkmann, J. Chem. Phys. 138 (2013) 064201.
[8] I.M. Haies, J.A. Jarvis, H. Bentley, I. Heinmaa, I. Kuprov, P.T.F. Williamson, M. Carravetta, Phys. Chem. Chem. Phys. 17 (2015) 6577–6587.
[9] A.J. Rossini, L. Emsley, L.A. O'Dell, Phys. Chem. Chem. Phys. 16 (2014) 12890–12899.
[10] I.M. Haies, J.A. Jarvis, L.J. Brown, I. Kuprov, P.T.F. Williamson, M. Carravetta, Phys. Chem. Chem. Phys. 17 (2015) 23748–23753.
[11] Z. Gan, J. Am. Chem. Soc. 128 (2006) 6040–6041.
[12] S. Cavadini, A. Lupulescu, S. Antonijevic, G. Bodenhausen, J. Am. Chem. Soc. 128 (2006) 7706–7707.
[13] S. Cavadini, Prog. Nucl. Magn. Reson. Spec. 56 (2010) 46–77.
[14] Y. Nishiyama, M. Malon, Z. Gan, Y. Endo, T. Nemoto, J. Magn. Reson. 230 (2013) 160–164.
[15] L.A. O'Dell, R. He, J. Pandohee, Cryst. Eng. Comm. 15 (2013) 8657–8667.
[16] L.A. O'Dell, Ann. Rep. NMR Spec. 86 (2015) 211–236.
[17] M. Shen, J. Trébosc, L.A. O'Dell, O. Lafon, F. Pourpoint, B. Hu, Q. Chen, J.-P. Amoureux, J. Magn. Reson. 258 (2015) 86–95.
[18] E. Kupče, R. Freeman, J. Magn. Reson. A 115 (1995) 273–276.
[19] L.A. O'Dell, Solid State Nucl. Magn. Reson. 55–56 (2013) 28–41.
[20] D.-K. Lee, A. Ramamoorthy, Chem. Phys. Lett. 280 (1997) 501–506.
[21] M. Shen, Q. Chen, J.-P. Amoureux, B. Hu, Solid State Nucl. Magn. Reson. 78 (2016) 5–8.

[22] K. Takegoshi, K. Hikichi, Chem. Phys. Lett. 194 (1992) 359–362.
[23] L. Marinelli, S. Wi, L. Frydman, J. Chem. Phys. 110 (1999) 3100–3112.
[24] N.M. Trease, P.J. Grandinetti, J. Chem. Phys. 128 (2008) 052318.
[25] M. Edén, Y.K. Lee, M.H. Levitt, J. Magn. Reson. A 120 (1996) 56–71.
[26] H. Conroy, J. Chem. Phys. 47 (1967) 5307–5318.
[27] M. Bak, J.T. Rasmussen, N.C. Nielsen, J. Magn. Reson. 147 (2000) 296–330.
[28] D.I. Hoult, R.E. Richards, J. Magn. Reson. 24 (1976) 71–85.